



CHORUS

This is the accepted manuscript made available via CHORUS. The article has been published as:

Magnetism driven by the interplay of fluctuations and frustration in the easy-axis triangular XXZ model with transverse fields

Daisuke Yamamoto, Giacomo Marmorini, Masahiro Tabata, Kazuki Sakakura, and Ippei Danshita

Phys. Rev. B **100**, 140410 — Published 21 October 2019

DOI: [10.1103/PhysRevB.100.140410](https://doi.org/10.1103/PhysRevB.100.140410)

Magnetism Driven by the Interplay of Fluctuations and Frustration in the Easy-Axis Triangular XXZ Model with Transverse Fields

Daisuke Yamamoto,¹ Giacomo Marmorini,² Masahiro Tabata,¹ Kazuki Sakakura,¹ and Ippei Danshita³

¹*Department of Physics and Mathematics, Aoyama Gakuin University, Sagamihara, Kanagawa 252-5258, Japan*

²*Research and Education Center for Natural Sciences,*

Keio University, Kanagawa 223-8521, Japan and

³*Department of Physics, Kindai University, Higashi-Osaka, Osaka 577-8502, Japan*

(Dated: September 9, 2019)

We study the combined effects of fluctuations and frustration in frustrated antiferromagnets described by the spin-1/2 easy-axis XXZ model with transverse magnetic fields, and propose its promising quantum simulation with a coherently coupled binary mixture of Fermi atoms in a triangular optical lattice. We perform a cluster mean-field plus scaling analysis to show that the ground state exhibits several nontrivial magnetic phases and a spin reorientation transition caused by the quantum order-by-disorder mechanism. Moreover, we find from Monte Carlo simulations that thermal fluctuations induce an unexpected coexistence of Berezinskii-Kosterlitz-Thouless physics and long-range order in different correlators. These predictions, besides being relevant to present and future experiments on triangular antiferromagnetic materials, can be tested in the laboratory with the combination of the currently available techniques for cold atoms.

Introduction.— Quantum simulations of solid materials with more flexible systems based on cold atomic gases have attracted increasing attention as the third platform to complement the conventional theoretical and experimental studies^{1–3}. In particular, a binary mixture of Fermi atoms in an optical lattice^{4–13} is a promising candidate to simulate the Hubbard model that describes strongly correlated electrons in solids. Although Fermi gases used to suffer from a technical difficulty in cooling to the regime of magnetic ordering, that is being overcome by recent innovative experimental^{5,10,14} and theoretical^{15–18} efforts. There has also been rapid development in detection techniques of quantum states, especially imaging individual atoms by the quantum gas microscope (QGM)^{7–12}. Owing to them, the observations of dimerized⁴, short-ranged^{5–9,12}, string¹¹ and $SU(\mathcal{N})$ ¹³ spin correlations have been achieved in the past few years. Mazurenko *et al.* reached the low temperatures at which the magnetic correlation length exceeded the linear size of their synthetic system made of two-component Fermi gases in a square optical lattice¹⁰.

In this Rapid Communication, we make a proposal and provide the necessary theoretical modeling to push the boundaries of cold-atom simulation towards the study of a more challenging issue, namely quantum frustrated magnetism. Motivated by the success of Ref. 10, we suggest a synthetic Hubbard system of binary Fermi gases in a triangular optical lattice for studying the frustrated magnetism deeply connected to the ongoing experiments on quasi-two-dimensional (quasi-2D) layered materials of quantum triangular-lattice antiferromagnets (TLAFs)^{19–30}. Here we consider a synthetic TLAF in the physically interesting parameter space defined by the spin-exchange anisotropy of easy-axis type and the magnetic field applied perpendicular to the anisotropy axis. Note that, whereas a classical triangular antiferromagnetic XY model has been created in cold gases of bosonic atoms³¹, there has been no realization of a quantum

TLAF or even a classical one with easy-axis anisotropy.

From the standpoint of real materials, only very few available compounds have an equilateral triangular-lattice structure with quantum spin $S = 1/2$ ^{20–23,25–27,30} and they typically do not fall into the range of easy-axis anisotropy (with the possible exception of $Ba_3CoNb_2O_9$ ²⁶). On the theoretical side, the interplay of quantum or thermal fluctuations and geometrical frustration in our proposed system with no $U(1)$ spin-rotational symmetry is an open problem. The lack of symmetry inhibits the decomposition of the Hilbert space, making numerical calculations with, e.g., exact diagonalization and density matrix renormalization group (DMRG) even more difficult in 2D or higher. Besides, the quantum Monte Carlo (QMC) method suffers from the notorious minus-sign problem³². To overcome this numerical challenge, here we develop a new framework of the cluster mean-field method combined with a scaling analysis (CMF+S)^{33–35} by employing the 2D DMRG algorithm as a cluster solver. Of particular interest is the drastic change in the quantum phase diagram from the classical one due to the order-by-disorder phenomena, which has been poorly studied so far because of the lack of the suitable methods.

We find that a particular quantum selection of the ground state gives rise to a novel gradual reorientation of three-sublattice magnetic orders, in addition to the stabilization of nonclassical phases in a wide region of the quantum phase diagram. Furthermore, performing classical Monte Carlo simulations to investigate thermal fluctuations, we show that the paramagnetic transition exhibits a two-step behavior through an intermediate phase with an unexpected coexistence of Berezinskii-Kosterlitz-Thouless (BKT) physics and long-range order (LRO) in different correlators. Our theoretical phase diagrams are meant to play a role in the two-way relationship which characterizes this early stage of the quantum simulation of frustrated physics: on the one hand, they act

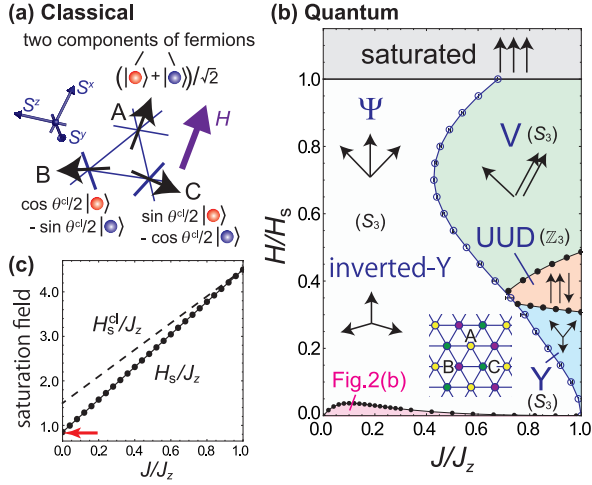


FIG. 1: Emergence of various quantum magnetic phases [(b)] due to quantum fluctuation effects on the classical-spin state [(a)]. The curves with open (filled) circles indicate first- (second-) order transitions. The broken symmetry in each phase (for $J/J_z < 1$) is indicated in parentheses. (c) Classical (H_s^{cl}) and Quantum (H_s) values of the saturation field strength. The red arrow in (c) marks the estimation $H_s/J_z = 0.825 \pm 0.025$ of Ref. 49 for the transverse Ising model.

as a benchmark for future cold-atom experiments; on the other hand, they can and must be checked with the help of the quantum simulator.

Synthetic spin-1/2 transverse XXZ system.— The system of coherently coupled Fermi mixtures of two hyperfine states ($\sigma = \uparrow, \downarrow$) is described by the Hamiltonian

$$\hat{\mathcal{H}} = - \sum_{\langle i,j \rangle, \sigma} t_{\sigma} \left(\hat{c}_{i\sigma}^{\dagger} \hat{c}_{j\sigma} + \text{H.c.} \right) + U \sum_i \hat{n}_{i\uparrow} \hat{n}_{i\downarrow} + \frac{\Omega}{2} \sum_i \left(\hat{c}_{i\uparrow}^{\dagger} \hat{c}_{i\downarrow} + \hat{c}_{i\downarrow}^{\dagger} \hat{c}_{i\uparrow} \right). \quad (1)$$

In addition to the preparation of triangular optical lattice^{36,37}, the ingredients of this Hamiltonian can be engineered in the laboratory by state-dependent optical lattices^{38–40} (for $t_{\uparrow} \neq t_{\downarrow}$) and by coherent couplings between two hyperfine states with Raman laser beams or radio-frequency field created in an atom chip^{41,42} (for Ω). The frustrated magnetism for dominant interactions ($U/t_{\sigma} \gg 1$)⁴³ is described by

$$\hat{\mathcal{H}} = \sum_{\langle i,j \rangle} \left(J \hat{S}_i^x \hat{S}_j^x + J \hat{S}_i^y \hat{S}_j^y + J_z \hat{S}_i^z \hat{S}_j^z \right) - H \sum_i \hat{S}_i^x, \quad (2)$$

where $\hat{S}_i^{\alpha} = \sum_{\sigma\sigma'} \hat{c}_{i\sigma}^{\dagger} \sigma_{\sigma\sigma}^{\alpha} \hat{c}_{i\sigma'}/2$ with the Pauli matrices σ^{α} plays the role of quantum spin $S = 1/2$. The anisotropy in the spin exchange interactions $J = 4t_{\uparrow}t_{\downarrow}/U$ and $J_z = 2(t_{\uparrow}^2 + t_{\downarrow}^2)/U$ must be of easy-axis type ($J \leq J_z$). The control of the Rabi frequency translates into tuning a transverse magnetic field, $H = -\Omega$ ⁴⁴.

Classical spins.— By treating the spins as classical vectors $\mathbf{S}_i = (\sin \theta_i \cos \varphi_i, \sin \theta_i \sin \varphi_i, \cos \theta_i)/2$, one gets the

classical (mean-field) energy of the system (2). Its minimization with respect to the spin angles θ_i and φ_i leads to a three-sublattice $\sqrt{3} \times \sqrt{3}$ coplanar order in which the polar angles on the sublattices $\mu = A, B$, and C are given by $\theta_A = \pi/2$, $\theta_B = \pi - \theta_C = \theta^{\text{cl}} \equiv \arcsin \frac{2H/3 - J}{J + J_z}$ while the azimuthal angles are $\varphi_A = 0$ and $\varphi_B = \varphi_C = \pi$ for $0 < H < 3J/2$ and $\varphi_A = \varphi_B = \varphi_C = 0$ for $3J/2 < H < H_s^{\text{cl}} \equiv 3J + 3J_z/2$. The ground state has a six-fold degeneracy corresponding to the sublattice exchange and resulting in a S_3 symmetry breaking. As illustrated in Fig. 1(a), the sublattice magnetic moments form an inverted-Y (resp. Ψ) shape for low (resp. high) magnetic fields. The inverted-Y and Ψ states are continuously connected and thus equivalent. Therefore, the classical ground state experiences no phase transition up to the magnetic saturation at $H = H_s^{\text{cl}}$.

Quantum phase diagram.— The numerical CMF+S method^{33–35} with 2D DMRG solver is used to unveil quantum fluctuation effects on the classical ground state. We consider a triangular-shaped cluster of N_C ($= 3, 6, 15, 21, 36$) spins placed in the environment of self-consistent mean fields ($Jm_{\mu}^x, Jm_{\mu}^y, J_z m_{\mu}^z$). The sublattice magnetic moments m_{μ}^{α} characterize the magnetic order. The CMF+S calculations permit the systematic inclusion of quantum-fluctuation effects by increasing N_C , which connects between the classical ($N_C = 1$) and exactly quantum ($N_C \rightarrow \infty$) regimes. The use of the 2D DMRG solver instead of the Lanczos diagonalization employed in the previous works^{33–35} considerably enlarges the tractable cluster size N_C ⁴⁵.

The quantum phase diagram is shown in Fig. 1(b). It surprisingly reveals various ground states that are absent in the classical counterpart. First, the sequence of the three magnetic phases – coplanar Y-shaped state, collinear up-up-down (UUD) state, and coplanar V-shaped state – is stabilized from low to high fields in the region bounded by the first-order transition line. Although the quantum-stabilized Y state is equivalent to the inverted-Y state in terms of symmetry breaking, one of the sublattice magnetic moments points in the opposite direction to the magnetic field. This quantum stabilization has been studied for the isotropic ($J/J_z = 1$) case^{46–48}: The correction to the energy due to the zero-point quantum fluctuations selects the Y-UUD-V sequence from the large classical ground-state manifold⁴⁶, resulting in the formation of the magnetization plateau of the UUD phase^{46–48}. Figure 1(b) shows that this quantum effect actually spreads over a wide region of J/J_z , especially for high magnetic fields. The phase boundaries have been determined by extrapolating the results of $N_C = 15, 21$, and 36 ⁴⁵.

Although the three sublattice moments in the UUD state are collinear along the field direction in the expectation values, the $U(1)$ spin rotational symmetry is absent for $J/J_z < 1$ [due to $\sum_i [\hat{S}_i^x, \hat{\mathcal{H}}] \neq 0$] in the full quantum-mechanical sense. Thus, the magnetization plateau is not exactly flat, although the slope is quite small [see Fig. 2(a)]. For the same reason, the saturation field H_s

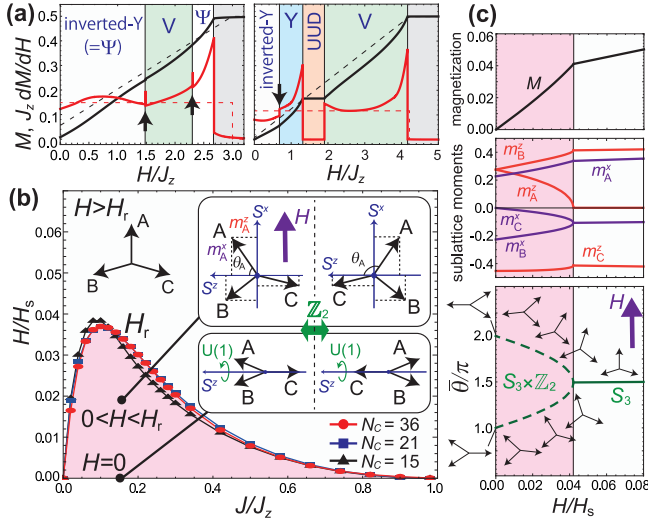


FIG. 2: (a) Magnetization curve $M(H) = (m_A^x + m_B^x + m_C^x)/3$ and its field derivative $J_z dM/dH$ for $J/J_z = 0.5$ (left) and $J/J_z = 0.906$ (right). The CMF+S results (solid lines) are compared to the classical-spin analysis (dashed lines). The arrows indicate the locations of first-order transitions. (b) Novel spin reorientation transition in the enlarged view of the low-field region of Fig. 1(b). The pairs of the \mathbb{Z}_2 degenerate states are illustrated in the insets. Besides, the exchange of the sublattice indices A, B, C is possible in the S_3 manifold. (c) Magnetization curve, the sublattice moments for one of the states in the degenerate manifold, and the values of $\bar{\theta}$ along $J/J_z = 0.3$.

is affected by quantum fluctuations and reduced from the classical value H_s^{cl} except at $J/J_z = 1$, as shown in Fig. 1(c). As shown in Fig. 2(a), the magnetization process exhibits a reentrant behavior for $0.43 \lesssim J/J_z \lesssim 0.68$ from the inverted-Y ($=\Psi$) to V and back to Ψ state.

Fluctuation-driven spin reorientation.— Even more interestingly, we find the emergence of a novel spin-reorientation transition in the low-field region of the quantum phase diagram [see Fig. 2(b)]. This stems from a quantum order-by-disorder selection from another non-trivial degenerate manifold of the classical ground state at $H = 0$, which has the topology of $S^1 \times S^{150-52}$. Quantum fluctuations select a specific Y-shape order in which one sublattice spin moment is directed parallel to the easy axis, as illustrated in Fig. 2(b); this agrees with the prediction of the linear spin-wave approximation⁵².

When a transverse field H is applied, a generic three-sublattice state breaks a $S_3 \times \mathbb{Z}_2$ symmetry (corresponding to the permutation of sublattice indices and the reflection about the field axis). Our CMF+S analysis shows that a quantum phase that indeed breaks such symmetry completely is realized with a coplanar spin order in the S^z - S^x plane [see Figs. 2(b) and 2(b)]. However, when H exceeds a threshold value H_r , the classical inverted-Y phase (which breaks S_3 symmetry) is recovered. Consequently, the structure of the sublattice moments is gradually changed from a Y shape to another Y shape with

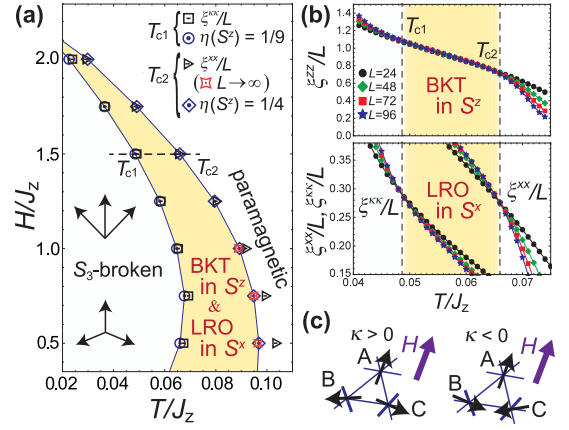


FIG. 3: (a) Thermal phase diagram for $J/J_z = 0.3$, obtained by the Monte Carlo simulations. (b) Scaled correlation lengths of the S^z - S^z , S^x - S^x , and chirality-chirality correlations at $H/J_z = 1.5$. (c) The inverted-Y states with positive and negative values of chirality.

different orientations via the intermediate $S_3 \times \mathbb{Z}_2$ -broken phase, which does not occur in the classical case. The behavior of this reorientation transition can be characterized by a parameter $\bar{\theta} \equiv \theta_A + \theta_B + \theta_C$, which is independent of the sublattice exchange. The two branches in the bottom panel of Fig. 2(c), one of which is spontaneously chosen, correspond to the remaining \mathbb{Z}_2 degeneracy.

Thermodynamic phase diagram.— Finally, let us explore novel thermal-fluctuation effects and provide the estimation of the ordering transition temperature. We replace the spin operators in the Hamiltonian (2) with vectors \mathbf{S}_i of length 1/2 to perform classical Monte Carlo simulations on $L \times L$ rhombic clusters with $L = 24, 48, 72, 96$ under periodic boundary conditions⁴⁵. This is expected to provide a reasonable approximation away from the low-temperature quantum region.

The thermal phase diagram for the representative value $J/J_z = 0.3$ (away from the isotropic case^{53,54}) is summarized in Fig. 3. Supposing the inverted-Y order, we estimate the correlation length for the three-sublattice order in the S^z and S^x spin components (ξ^{zz} , ξ^{xx}) and for the uniform order in the y component of the vector chirality κ ($\xi^{\kappa\kappa}$) illustrated in Fig. 3(c). As shown in Fig. 3(b), ξ^{zz}/L exhibits a finite critical range, $T_{c1} < T < T_{c2}$, with a constant value independent of L , indicating a BKT phase with algebraic decay $\sim |\mathbf{r}_i - \mathbf{r}_j|^{-\eta}$ ^{55,56} of the S^z - S^z correlation function, despite the absence of continuous symmetry in the model (2). This can be explained from the discrete but high degree of degeneracy of the inverted-Y ground state; the critical exponent η at T_{c1} ($\sim 1/9$) and at T_{c2} ($\sim 1/4$) shown in Fig. 4(a) are indeed consistent with the expectation for the universality of the 2D 6-state clock model^{57,58}, whose \mathbb{Z}_6 symmetry group has six elements, same as the S_3 symmetry of the present case.

Coexistence of BKT and LRO.— Interestingly, however, ξ^{xx}/L and $\xi^{\kappa\kappa}/L$ show an isolated critical point,

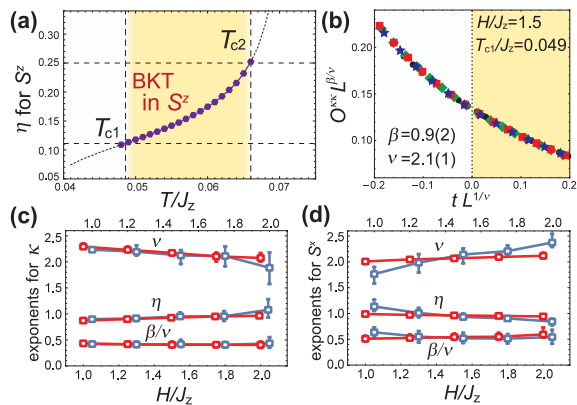


FIG. 4: (a) Critical exponent η for the S^z - S^z component. (b) Example of the scaling analyses on the chirality order parameter $\mathcal{O}^{\kappa\kappa}$ ⁴⁵ for the transition at T_{c1} . The extracted critical temperature is defined by $t \equiv (T - T_{c1})/T_{c1}$. The extracted critical exponents for the transitions at T_{c1} [(c)] and at T_{c2} [(d)] are plotted as a function of H/J_z . The scales of the upper and lower horizontal axes for the blue and red data points are slightly shifted from each other for convenience.

unlike ξ^{zz}/L , as seen in Fig. 3(b) as the crossings of the curves for different L ⁵⁹. The critical points for S^x and κ are coincident or very close to the upper and lower endpoints of the BKT behavior in S^z , respectively. Consequently, in the intermediate phase for $T_{c1} < T < T_{c2}$, BKT-type quasi-LRO in the field-perpendicular component (S^z) and LRO in the field-parallel component (S^x) coexist while the chirality is disordered. This particular coexistence of BKT and LRO should be attributed to the difference of S_3 from \mathbb{Z}_6 ; the nonabelian symmetric group S_3 is formed by the cycles and transpositions of $\{A, B, C\}$ and has two generators, while \mathbb{Z}_6 is just formed by the cycles of six elements and has one generator. In fact, the breaking of the even and odd permutation symmetries is detected by S^x and κ , respectively. The S^x component of the magnetic moments in the inverted-Y order takes the same value on two of the three sublattices, and thus all exchanges generating three elements can be obtained only by cyclic permutations of the sublattice indices while the chirality changes its sign by transposing two sublattice indices.

Possible new universality class.— It is noteworthy that the critical exponents associated with diverging ξ^{xx} and $\xi^{\kappa\kappa}$ have no correspondence in the known universality classes. From the standard scaling analyses⁴⁵, we extract the values of the correlation-function (η), order-parameter (β), and correlation-length (ν) exponents for the transitions in S^x at T_{c2} and in κ at T_{c1} , respectively [see Figs. 4(b-d)]. The blue and red symbols in Figs. 4(c) and (d) are the critical exponents extracted with two different ways to estimate T_{c2} (T_{c1}), namely from the crossings in the scaled correlation length ξ^{xx}/L ($\xi^{\kappa\kappa}/L$) and from the condition $\eta = 1/4$ ($\eta = 1/9$) for the S^z correlation function. Note that the latter estimation of the critical points has less finite-size effect. As shown

in Fig. 4(d), the values of η and β/ν for S^x are roughly constant (at ~ 1 and ~ 0.5) for varying H/J_z , preserving the 2D hyperscaling law $\eta = 2\beta/\nu$, which indicates the existence of a new weak universality⁶⁰. Moreover, the individual exponents β and ν might also be constant (implying a new universality in the usual sense), although we cannot reach a final conclusion with the given numerical data. The critical exponents associated with the chiral transition at T_{c1} also have a similar behavior as shown in Fig. 4(c). In both transitions at T_{c2} and T_{c1} , the critical exponents are clearly distinguished from the naively expected 2D three-state Potts ($\eta = 4/15$, $\beta = 1/9$, $\nu = 5/6$) and Ising ($\eta = 1/4$, $\beta = 1/8$, $\nu = 1$) ones, which means that the two-step transition and the emergent BKT-LRO coexistence are not a simple sequence of standard \mathbb{Z}_3 and \mathbb{Z}_2 symmetry breaking transitions.

Conclusions.— We studied the quantum and thermal phase transitions in the easy-axis triangular XXZ model under transverse magnetic fields and proposed their quantum simulation with coherently-coupled binary gases of ultracold fermionic atoms. In the ground state, the order-by-disorder effects induced by the quantum fluctuations give rise to several nontrivial phase transitions, including a novel spin reorientation. Moreover, the transition from the paramagnetic to the ordered state with S_3 symmetry breaking was found to exhibit a particular two-step behavior via an intermediate phase with coexisting BKT and LRO correlations. The temperature scale of the transitions was estimated from the Monte Carlo analysis to be at most of order $0.1J_z$ [see Fig. 3(a)], with little sensitivity to the variation of J/J_z . With the caveat that quantum fluctuations can actually lower this temperature to some extent, this estimation should serve as a reference for future cold-atom quantum simulation of novel frustrated magnetism.

The different magnetically ordered phases found here could be detected by the QGM⁷⁻¹². As well as the S^z components, it is also possible to measure the transverse components by inserting a radiofrequency pulse that rotates the spins by $\pi/2$ ^{12,61}. For finite-size optical lattice systems, the order parameter and the correlation length for each phase can be extracted from the structure factor for the corresponding spin component and wavevector, which is obtained by gathering many QGM shots, just like in the Monte Carlo simulations⁴⁵.

In addition, very recently, a two-step thermal transition has been observed in the easy-axis TLAf compound $\text{Ba}_2\text{La}_2\text{NiTe}_2\text{O}_{12}$ ⁶². Although the anisotropy is of single-ion type, the physics is expected to be deeply related to the present system, and thus it should be interesting to apply transverse fields to single crystals of that material.

Finally, we emphasize that using a 2D DMRG solver within the CMF+S scheme significantly expands the scope of the method to broader areas of quantum frustrated systems, thanks to the tractability of series of larger clusters.

Acknowledgments

This work was supported by KAKENHI from Japan Society for the Promotion of Science, Grant Numbers 18K03525 (D.Y.), 18K03492 (I.D.), 18H05228 (I.D.), and CREST from Japan Science and Technology Agency No. JPMJCR1673. G.M. wants to thank P. Calabrese,

E. Vicari and W. Vinci for useful correspondence. G.M. is supported by the Ministry of Education, Culture, Sports, Science (MEXT)-Supported Program for the Strategic Research Foundation at Private Universities “Topological Science” (Grant No. S1511006). Part of the calculations was carried out using the TSC computer of the “Topological Science” project in Keio University.

-
- ¹ M. Lewenstein, A. Sanpera, V. Ahufinger, B. Damski, A. Sen(De), and U. Sen, *Adv. Phys.* **56**, 243 (2007).
- ² I. Bloch, J. Dalibard, and S. Nascimbene, *Nat. Phys.* **8**, 267 (2012).
- ³ C. Gross and I. Bloch, *Science* **357**, 995 (2017).
- ⁴ D. Greif, T. Uehlinger, G. Jotzu, L. Tarruell, and T. Esslinger, *Science* **340**, 1307 (2013).
- ⁵ R. A. Hart, P. M. Duarte, T.-L. Yang, X. Liu, T. Paiva, E. Khatami, R. T. Scalettar, N. Trivedi, D. A. Huse, and R. G. Hulet, *Nature (London)* **519**, 211 (2015).
- ⁶ D. Greif, G. Jotzu, M. Messer, R. Desbuquois, and T. Esslinger, *Phys. Rev. Lett.* **115**, 260401 (2015).
- ⁷ M. F. Parsons, A. Mazurenko, C. S. Chiu, G. Ji, D. Greif, and M. Greiner, *Science* **353**, 1253 (2016).
- ⁸ M. Boll, T. A. Hilker, G. Salomon, A. Omran, J. Nespolo, L. Pollet, I. Bloch, and C. Gross, *Science* **353**, 1257 (2016).
- ⁹ L. W. Cheuk, M. A. Nichols, K. R. Lawrence, M. Okan, H. Zhang, E. Khatami, N. Trivedi, T. Paiva, M. Rigol, and M. W. Zwierlein, *Science* **353**, 1260 (2016).
- ¹⁰ A. Mazurenko, C. S. Chiu, G. Ji, M. F. Parsons, M. Kanász-Nagy, R. Schmidt, F. Grusdt, E. Demler, D. Greif, and M. Greiner, *Nature (London)* **545**, 462 (2017).
- ¹¹ T. A. Hilker, G. Salomon, F. Grusdt, A. Omran, M. Boll, E. Demler, I. Bloch, and C. Gross, *Science* **357**, 484 (2017).
- ¹² P. T. Brown, D. Mitra, E. Guardado-Sanchez, P. Schauß, S. S. Kondov, E. Khatami, T. Paiva, N. Trivedi, D. A. Huse, and W. S. Bakr, *Science* **357**, 1385 (2017).
- ¹³ H. Ozawa, S. Taie, Y. Takasu, and Y. Takahashi, *Phys. Rev. Lett.* **121**, 225303 (2018).
- ¹⁴ S. Taie, R. Yamazaki, S. Sugawa, and Y. Takahashi, *Nat. Phys.* **8**, 825 (2012).
- ¹⁵ J.-S. Bernier, C. Kollath, A. Georges, L. De Leo, F. Gerbier, C. Salomon, and M. Köhl, *Phys. Rev. A* **79**, 061601(R) (2009).
- ¹⁶ C. J. M. Mathy, D. A. Huse, and R. G. Hulet, *Phys. Rev. A* **86**, 023606 (2012).
- ¹⁷ A. Kantian, S. Langer, and A. J. Daley, *Phys. Rev. Lett.* **120**, 060401 (2018).
- ¹⁸ S. Goto and I. Danshita, *Phys. Rev. A* **96**, 063602 (2017).
- ¹⁹ R. Ishii, S. Tanaka, K. Onuma, Y. Nambu, M. Tokunaga, T. Sakakibara, N. Kawashima, Y. Maeno, C. Broholm, D. P. Gautreaux, *Europhys. Lett.* **94**, 17001 (2011).
- ²⁰ Y. Shirata, H. Tanaka, A. Matsuo, and K. Kindo, *Phys. Rev. Lett.* **108**, 057205 (2012).
- ²¹ H. D. Zhou, C. Xu, A. M. Hallas, H. J. Silverstein, C. R. Wiebe, I. Umegaki, J. Q. Yan, T. P. Murphy, J.-H. Park, Y. Qiu, J. R. D. Copley, J. S. Gardner, and Y. Takano, *Phys. Rev. Lett.* **109**, 267206 (2012).
- ²² T. Susuki, N. Kurita, T. Tanaka, H. Nojiri, A. Matsuo, K. Kindo, and H. Tanaka, *Phys. Rev. Lett.* **110**, 267201 (2013).
- ²³ M. Lee, J. Hwang, E. S. Choi, J. Ma, C. R. Dela Cruz, M. Zhu, X. Ke, Z. L. Dun, and H. D. Zhou, *Phys. Rev. B* **89**, 104420 (2014).
- ²⁴ M. Lee, E. S. Choi, X. Huang, J. Ma, C. R. Dela Cruz, M. Matsuda, W. Tian, Z. L. Dun, S. Dong, and H. D. Zhou, *Phys. Rev. B* **90**, 224402 (2014).
- ²⁵ D. Yamamoto, G. Marmorini, and I. Danshita, *Phys. Rev. Lett.* **114**, 027201 (2015).
- ²⁶ K. Yokota, N. Kurita, and H. Tanaka, *Phys. Rev. B* **90**, 014403 (2014).
- ²⁷ G. Koutroulakis, T. Zhou, Y. Kamiya, J. D. Thompson, H. D. Zhou, C. D. Batista, and S. E. Brown, *Phys. Rev. B* **91**, 024410 (2015).
- ²⁸ S. Ito, N. Kurita, H. Tanaka, S. Ohira-Kawamura, K. Nakajima, S. Itoh, K. Kuwahara, and K. Kakurai, *Nat. Commun.* **8**, 235 (2017).
- ²⁹ J. A. M. Paddison, M. Daum, Z. L. Dun, G. Ehlers, Y. Liu, M. B. Stone, H. D. Zhou, and M. Mourigal, *Nat. Phys.* **13**, 117 (2017).
- ³⁰ Y. Cui, J. Dai, P. Zhou, P. S. Wang, T. R. Li, W. H. Song, J. C. Wang, L. Ma, Z. Zhang, S. Y. Li, G. M. Luke, B. Normand, T. Xiang, and W. Yu, *Phys. Rev. Materials* **2**, 044403 (2018).
- ³¹ J. Struck, C. Ölschläger, R. Le Targat, P. Soltan-Panahi, A. Eckardt, M. Lewenstein, P. Windpassinger, and K. Sengstock, *Science* **333**, 996 (2011).
- ³² M. Suzuki, *Quantum Monte Carlo Methods in Condensed Matter Physics* (World Scientific, Singapore, 1993).
- ³³ D. Yamamoto, A. Masaki, and I. Danshita, *Phys. Rev. B* **86**, 054516 (2012).
- ³⁴ D. Yamamoto, G. Marmorini, and I. Danshita, *Phys. Rev. Lett.* **112**, 127203 (2014); *ibid.*, **112**, 259901 (2014).
- ³⁵ D. Yamamoto, H. Ueda, I. Danshita, G. Marmorini, T. Momoi, and T. Shimokawa, *Phys. Rev. B* **96**, 014431 (2017).
- ³⁶ C. Becker, P. Soltan-Panahi, J. Kronjäger, S. Dörscher, K. Bongs, and K. Sengstock, *New J. Phys.* **12**, 065025 (2010).
- ³⁷ C. K. Thomas, T. H. Barter, T.-H. Leung, M. Okano, G.-B. Jo, J. Guzman, I. Kimchi, A. Vishwanath, and D. M. Stamper-Kurn, *Phys. Rev. Lett.* **119**, 100402 (2017).
- ³⁸ O. Mandel, M. Greiner, A. Widera, T. Rom, T. W. Hänsch, and I. Bloch, *Phys. Rev. Lett.* **91**, 010407 (2003).
- ³⁹ P. J. Lee, M. Anderlini, B. L. Brown, J. Sebby-Strabley, W. D. Phillips, and J. V. Porto, *Phys. Rev. Lett.* **99**, 020402 (2007).
- ⁴⁰ G. Jotzu, M. Messer, F. Görg, D. Greif, R. Desbuquois, and T. Esslinger, *Phys. Rev. Lett.* **115**, 073002 (2015).
- ⁴¹ N. Goldman, I. Satija, P. Nikolic, A. Bermudez, M. A. Martin-Delgado, M. Lewenstein, and I. B. Spielman, *Phys. Rev. Lett.* **105**, 255302 (2010).
- ⁴² B. M. Anderson, I. B. Spielman, and G. Juzeliūnas, *Phys. Rev. Lett.* **111**, 125301 (2013).
- ⁴³ A. B. Kuklov and B. V. Svistunov, *Phys. Rev. Lett.* **90**, 100401 (2003).

- ⁴⁴ D. Jakscha and P. Zoller, *Annals of Physics* **315**, 52 (2005).
- ⁴⁵ See Supplemental Material at [http:\[URL\]](http://[URL]) for technical details.
- ⁴⁶ A. V. Chubukov and D. I. Golosov, *J. Phys.: Condens. Matter* **3**, 69 (1991).
- ⁴⁷ A. Honecker, J. Schulenburg, and J. Richter, *J. Phys. Condens. Matter* **16**, S749 (2004).
- ⁴⁸ T. Sakai and H. Nakano, *Phys. Rev. B* **83**, 100405(R) (2011).
- ⁴⁹ S. V. Isakov and R. Moessner, *Phys. Rev. B* **68**, 104409 (2003).
- ⁵⁰ S. Miyashita and H. Kawamura, *J. Phys. Soc. Jpn.* **54**, 3385 (1985).
- ⁵¹ S. Miyashita, *J. Phys. Soc. Jpn.* **55**, 3605 (1986).
- ⁵² Q. Sheng and C. L. Henley, *J. Phys. Cond. Matt.* **4** 2937 (1992).
- ⁵³ H. Kawamura and S. Miyashita, *J. Phys. Soc. Jpn.* **54**, 4530 (1985).
- ⁵⁴ L. Seabra, T. Momoi, P. Sindzingre, and N. Shannon, *Phys. Rev. B* **84**, 214418 (2011).
- ⁵⁵ H. G. Katzgraber, M. Körner, and A. P. Young, *Phys. Rev. B* **73**, 224432 (2006).
- ⁵⁶ T. Surungan, S. Masuda, Y. Komura, and Y. Okabe, *J. Phys. A: Math. Theor.* **52** 275002 (2019).
- ⁵⁷ J. V. Jose, L. P. Kadanoff, S. Kirkpatrick, and D.R. Nelson, *Phys. Rev. B* **16**, 1217 (1977).
- ⁵⁸ K. Damle, *Phys. Rev. Lett.* **115**, 127204 (2015).
- ⁵⁹ A. W. Sandvik, *AIP Conf. Proc.* **1297**, 135 (2010).
- ⁶⁰ M. Suzuki, *Prog. Theor. Phys.* **51**, 1992 (1974).
- ⁶¹ C. D. Hamley, C. S. Gerving, T. M. Hoang, E. M. Bookjans, and M. S. Chapman, *Nat. Phys.* **8**, 305 (2012).
- ⁶² M. Saito, M. Watanabe, N. Kurita, A. Matsuo, K. Kindo, M. Avdeev, H. O. Jeschke, and H. Tanaka, *Phys. Rev. B* **100**, 064417 (2019).